

The electroweak contribution to the top quark forward-backward asymmetry at the Tevatron

W. HOLLIK* and D. PAGANI†

Max-Planck-Institut für Physik
(Werner-Heisenberg-Institut)
D-80805 München, Germany

Abstract

The electroweak contributions to the forward-backward asymmetry in the production of top-quark pairs at the Tevatron are evaluated at $\mathcal{O}(\alpha^2)$ and $\mathcal{O}(\alpha\alpha_s^2)$. We perform a detailed analysis of all partonic channels that produce an asymmetry and combine them with the QCD contributions. They provide a non-negligible fraction of the QCD-induced asymmetry with the same overall sign, thus enlarging the Standard Model prediction and diminishing the observed deviation. For the observed mass-dependent forward-backward asymmetry a 3σ deviation still remains at an invariant-mass cut of $M_{t\bar{t}} > 450$ GeV.

*hollik@mppmu.mpg.de

†pagani@mppmu.mpg.de

1 Introduction

The investigation of the top quark at the Tevatron has substantially contributed to precision tests of QCD and the electroweak theory. Besides the valuable set of top-quark observables like mass, width, cross section, which are fully consistent with the SM, the measured forward-backward asymmetry A_{FB} of top-pair production [1, 2] is larger than expected from the Standard Model (SM) prediction and has led to speculations on the presence of possible new physics.

Two options for the forward-backward asymmetry have been used in the experimental analysis, with the definitions

$$A_{FB}^{t\bar{t}} = \frac{\sigma(\Delta y > 0) - \sigma(\Delta y < 0)}{\sigma(\Delta y > 0) + \sigma(\Delta y < 0)} \quad (1)$$

and

$$A_{FB}^{p\bar{p}} = \frac{\sigma(y_t > 0) - \sigma(y_t < 0)}{\sigma(y_t > 0) + \sigma(y_t < 0)} \quad (2)$$

given in [3] reporting the recent CDF result. Δy is defined as the difference between the rapidity y_t and $y_{\bar{t}}$ of t and \bar{t} where the proton direction defines the beam axis. Δy (not y_t) is invariant under a boost along the beam axis, thus it is the same in the partonic and in the hadronic rest frame.

The recent values for the inclusive asymmetry obtained by CDF [3] are

$$\begin{aligned} A_{FB}^{t\bar{t}} &= 0.158 \pm 0.075, \\ A_{FB}^{p\bar{p}} &= 0.150 \pm 0.055. \end{aligned} \quad (3)$$

The LO predictions of the Standard Model originate from NLO QCD contributions to the differential cross section for $t\bar{t}$ production that are antisymmetric under charge conjugation [4, 5], yielding values for $A_{FB}^{t\bar{t}}$ ($A_{FB}^{p\bar{p}}$) around 7%(5%) (see e.g. [6]). The observed difference between the measurement and the prediction has inspired quite a number of theoretical papers proposing various new physics mechanisms as potential additional sources for the forward-backward asymmetry (see for example [7, 8] and references therein).

The importance of identifying signals from possible new physics requires a thorough discussion of the SM prediction and the corresponding uncertainty. At present, the theoretical accuracy is limited by the missing NNLO contribution from QCD to the antisymmetric part of the $t\bar{t}$ production cross section. Besides the strong interaction, the electroweak interaction gives rise to further contributions to the $t\bar{t}$ forward-backward asymmetry, through photon and Z exchange at the tree level as well as through interference between QCD and electroweak amplitudes at NLO in both interactions. Although smaller in size, they are not negligible, and a careful investigation is an essential ingredient for an improved theoretical prediction.

In this paper we perform a detailed analysis of the electroweak contributions to the forward-backward asymmetry in $t\bar{t}$ production based on the evaluation of all partonic channels that produce an asymmetry both at the tree level and at NLO, and combine them with the QCD contributions. We apply the calculation to both types of asymmetries given above in (1) and (2). Moreover, we present results for $A_{FB}^{t\bar{t}}$ also with a cut $M_{t\bar{t}} > 450$ GeV on the invariant $t\bar{t}$ mass as well as with a rapidity cut $|\Delta y| > 1$, for comparison with the experimental values given in [3],

$$A_{FB}^{t\bar{t}}(M_{t\bar{t}} \geq 450 \text{ GeV}) = 0.475 \pm 0.114, \quad A_{FB}^{t\bar{t}}(|\Delta y| \geq 1) = 0.611 \pm 0.256, \quad (4)$$

where in particular the result for the high invariant-mass cut exhibits the largest deviation from the QCD prediction.

2 Computational basis

At leading order the production of $t\bar{t}$ pairs in $p\bar{p}$ collisions originates, via the strong interaction, from the partonic processes $q\bar{q} \rightarrow t\bar{t}$ and $gg \rightarrow t\bar{t}$, which yield the $\mathcal{O}(\alpha_s^2)$ of the (integrated) cross section, i.e. the denominator of A_{FB} in (1) and (2). The antisymmetric cross section, the numerator of A_{FB} , starts at $\mathcal{O}(\alpha_s^3)$ and gets contributions from $q\bar{q} \rightarrow t\bar{t}(g)$ with $q = u, d$ (the processes from other quark species, after convolution with the parton distributions and summation, are symmetric under $y_t \rightarrow -y_t$ and thus do not contribute to A_{FB}) as well as from $qg \rightarrow t\bar{t}q$ and $\bar{q}g \rightarrow t\bar{t}\bar{q}$.

Writing the numerator and the denominator of A_{FB} (for either of the definitions (1) and (2)) in powers of α_s we obtain

$$A_{FB} = \frac{N}{D} = \frac{\alpha_s^3 N_1 + \alpha_s^4 N_2 + \dots}{\alpha_s^2 D_0 + \alpha_s^3 D_1 + \dots} = \frac{\alpha_s}{D_0} (N_1 + \alpha_s (N_2 - N_1 D_1 / D_0)) + \dots \quad (5)$$

The terms up to one-loop (D_0, D_1, N_1) have been calculated [9, 10, 11, 12, 13, 14], [15, 16, 17, 18], [5], whereas only some parts of N_2 are currently known [19, 20]. The inclusion of the $N_1 D_1 / D_0$ term without N_2 would hence be incomplete, and we have chosen to use only the lowest order cross section in the denominator and the $\mathcal{O}(\alpha_s^3)$ term in the numerator, as done in [5].

Rewriting N and D to include the EW contributions yields the following expression for the leading terms,

$$A_{FB} = \frac{N}{D} = \frac{\alpha^2 \tilde{N}_0 + \alpha_s^3 N_1 + \alpha_s^2 \alpha \tilde{N}_1 + \alpha_s^4 N_2 + \dots}{\alpha^2 \tilde{D}_0 + \alpha_s^2 D_0 + \alpha_s^3 \tilde{D}_1 + \alpha_s^2 \alpha \tilde{D}_1 + \dots} = \alpha_s \frac{N_1}{D_0} + \alpha \frac{\tilde{N}_1}{D_0} + \frac{\alpha^2 \tilde{N}_0}{\alpha_s^2 D_0} + \dots \quad (6)$$

where the incomplete $\mathcal{O}(\alpha_s^2)$ part has been dropped. In the following we (re-)evaluate the three contributions on the r.h.s. of (6).

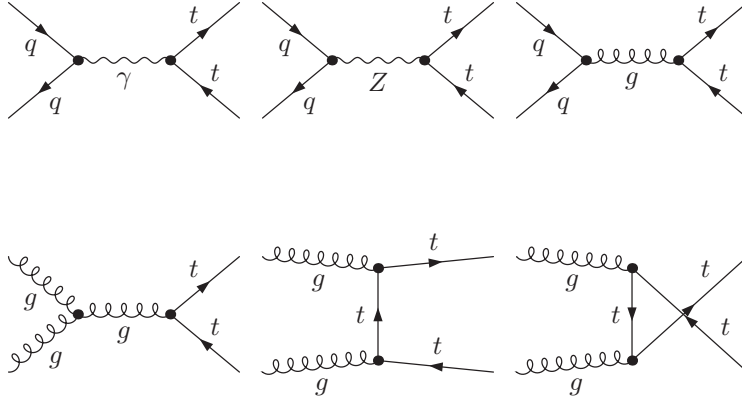


Figure 1: Electroweak and QCD Born diagrams

Figure 1 contains all the tree level diagrams for the partonic subprocesses $q\bar{q} \rightarrow t\bar{t}$ and $gg \rightarrow t\bar{t}$ (Higgs exchange is completely negligible). The squared terms $|\mathcal{M}_{q\bar{q} \rightarrow g \rightarrow t\bar{t}}|^2$ and $|\mathcal{M}_{g\bar{g} \rightarrow t\bar{t}}|^2$ yield

D_0 of the LO cross section; the $\mathcal{O}(\alpha^2)$ terms arise from $|\mathcal{M}_{q\bar{q}\rightarrow\gamma\rightarrow t\bar{t}} + \mathcal{M}_{q\bar{q}\rightarrow Z\rightarrow t\bar{t}}|^2$, which generate a purely-electroweak antisymmetric differential cross section, in the parton cms given by

$$\frac{d\sigma_{asym}}{d\cos\theta} = 2\pi\alpha^2 \cos\theta \left(1 - \frac{4m_t^2}{s}\right) \left[\kappa \frac{Q_q Q_t A_q A_t}{(s - M_Z^2)} + 2\kappa^2 A_q A_t V_q V_t \frac{s}{(s - M_Z^2)^2} \right], \quad (7)$$

$$\kappa = \frac{1}{4\sin^2(\theta_W)\cos^2(\theta_W)}, \quad V_q = T_q^3 - 2Q_q \sin^2(\theta_W), \quad A_q = T_q^3.$$

In A_{FB} (6) this leads to the term \tilde{N}_0 . The complementary symmetric cross section provides the \tilde{D}_0 term in the denominator, which does not contribute in the order under consideration. Interference of $q\bar{q} \rightarrow \gamma, Z \rightarrow t\bar{t}$ and $q\bar{q} \rightarrow g \rightarrow t\bar{t}$ is zero because of the color structure¹.

The $\mathcal{O}(\alpha_s^3)$ terms that contributes to N arise from four classes of partonic processes: $q\bar{q} \rightarrow t\bar{t}$, $q\bar{q} \rightarrow t\bar{t}g$, $qg \rightarrow t\bar{t}q$ and $\bar{q}g \rightarrow t\bar{t}\bar{q}$. In the first case the origin is the interference of QCD one-loop and Born amplitudes; the other processes correspond to real-particle emissions. All one-loop vertex

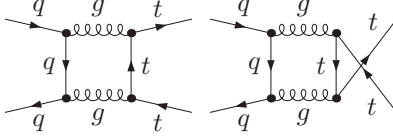


Figure 2: QCD box diagrams

corrections and self-energies do not generate any asymmetric term, hence only the box diagrams (Figure 2) are relevant. The box integrals are free of ultraviolet and collinear divergences, but they involve infrared singularities which are cancelled after adding the integrated real-gluon emission contribution $q\bar{q} \rightarrow t\bar{t}g$, shown in Figure 3. For the corresponding relevant gluon-radiation part only the interference of initial and final state gluon radiation has to be taken into account, yielding another antisymmetric cross section. The processes of real-quark radiation $qg \rightarrow t\bar{t}q$ and $\bar{q}g \rightarrow t\bar{t}\bar{q}$

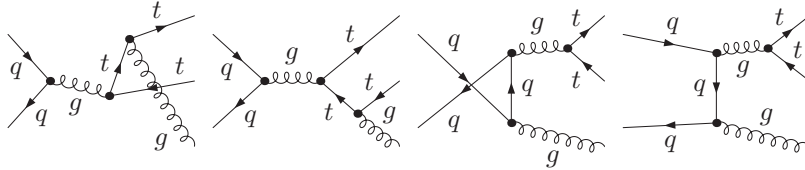


Figure 3: Real emission of gluons at $\mathcal{O}(\alpha_s^3)$

¹For $q\bar{q} \rightarrow t\bar{t}$ there are also $\mathcal{O}(\alpha)$ W -mediated t -channel diagrams with $q = d, s, b$, but they are strongly suppressed by the CKM matrix or by parton distributions ($q = b$).

yield contributions to A_{FB} which are numerically not important [5].

In order to analyze the electroweak $\mathcal{O}(\alpha_s^2\alpha)$ terms, it is useful to separate the QED contributions involving photons from the weak contributions with Z bosons. In the QED sector we obtain the $\mathcal{O}(\alpha_s^2\alpha)$ contributions to N from three classes of partonic processes: $q\bar{q} \rightarrow t\bar{t}$, $q\bar{q} \rightarrow t\bar{t}g$ and $q\bar{q} \rightarrow t\bar{t}\gamma$. The first case is the virtual-photon contribution, which can be obtained from the QCD analogue, namely the $\mathcal{O}(\alpha_s^3)$ interference of box and tree-level amplitudes, by substituting successively each one of the three internal gluons by a photon, as displayed in Figure 4.

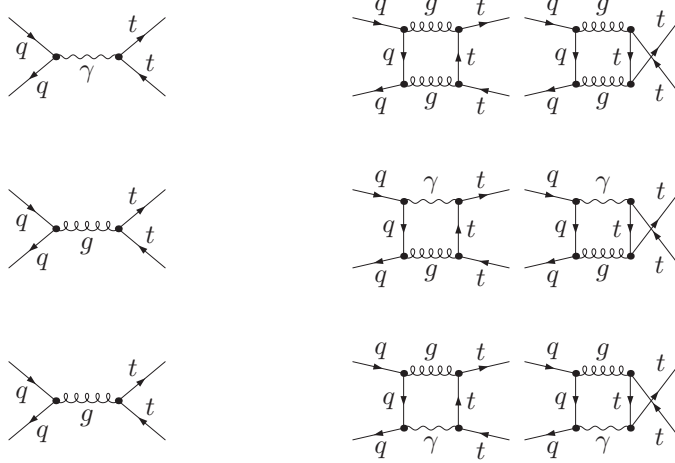


Figure 4: Different ways of QED–QCD interference at $\mathcal{O}(\alpha_s^2\alpha)$

The essential differences between the calculation of the $\mathcal{O}(\alpha_s^3)$ and of QED $\mathcal{O}(\alpha_s^2\alpha)$ terms are the coupling constants and the appearance of the $SU(3)$ generators in the strong vertices. Summing over color in the final state and averaging in the initial state we find for the virtual contributions to the antisymmetric cross section the following ratio,

$$\frac{\overline{|\mathcal{M}^{t\bar{t}}|}_{\mathcal{O}(\alpha_s^2\alpha), asym}^2}{\overline{|\mathcal{M}^{t\bar{t}}|}_{\mathcal{O}(\alpha_s^3), asym}^2} = \frac{2\text{Re}(\overline{\mathcal{M}^{t\bar{t}}}_{\mathcal{O}(\alpha)} \overline{\mathcal{M}^{t\bar{t}*}}_{\mathcal{O}(\alpha_s^2)})_{asym} + 2\text{Re}(\overline{\mathcal{M}^{t\bar{t}}}_{\mathcal{O}(\alpha_s)} \overline{\mathcal{M}^{t\bar{t}*}}_{\mathcal{O}(\alpha_s\alpha)})_{asym}}{2\text{Re}(\overline{\mathcal{M}^{t\bar{t}}}_{\mathcal{O}(\alpha_s)} \overline{\mathcal{M}^{t\bar{t}*}}_{\mathcal{O}(\alpha_s^2)})_{asym}} = \frac{F_{QED}^{t\bar{t}}(\alpha_s, \alpha, Q_t, Q_q)}{F_{QCD}^{t\bar{t}}(\alpha_s)} \quad (8)$$

that can be expressed in terms of two factors $F_{QED}^{t\bar{t}}$ and $F_{QCD}^{t\bar{t}}$ depending only on coupling constants and color traces,

$$F_{QCD}^{t\bar{t}} = \frac{g_s^6}{9} \delta_{AD} \delta_{BF} \delta_{EC} \text{Tr}(t^A t^B t^C) \left[\frac{1}{2} \text{Tr}(t^D t^E t^F) + \frac{1}{2} \text{Tr}(t^D t^F t^E) \right] = \frac{g_s^6}{16 \cdot 9} d^2, \quad (9a)$$

$$F_{QED}^{t\bar{t}} = n_{t\bar{t}} \left\{ \frac{g_s^4 e^2 Q_q Q_t}{9} \delta_{AC} \delta_{BD} \text{Tr}(t^A t^B) \text{Tr}(t^C t^D) \right\} = \frac{6g_s^4 e^2}{9} Q_t Q_q. \quad (9b)$$

$F_{QCD}^{t\bar{t}}$ contains two different color structures and the result depends on $d^2 = d^{ABC} d_{ABC} = \frac{40}{3}$, which arises from $\text{Tr}(t^A t^B t^C) = \frac{1}{4}(if^{ABC} + d^{ABC})$. $F_{QED}^{t\bar{t}}$ instead depends on the charges of the incoming quarks (Q_q) and of the top quark (Q_t), together with $n_{t\bar{t}} = 3$ corresponding to Figure 4.

In a similar way, also the real-radiation processes $q\bar{q} \rightarrow t\bar{t}g$ and $q\bar{q} \rightarrow t\bar{t}\gamma$ (Figures 5 and 6) can be evaluated starting from the result obtained for $q\bar{q} \rightarrow t\bar{t}g$ in the QCD case and substituting successively each gluon by a photon, yielding the ratios

$$\frac{\overline{|\mathcal{M}^{t\bar{t}g}|_{\mathcal{O}(\alpha_s^2\alpha),asym}^2}}{\overline{|\mathcal{M}^{t\bar{t}g}|_{\mathcal{O}(\alpha_s^3),asym}^2}} = \frac{2\text{Re}(\mathcal{M}_{\mathcal{O}(\alpha\sqrt{\alpha_s})}^{t\bar{t}g}\mathcal{M}_{\mathcal{O}(\alpha_s\sqrt{\alpha_s})}^{t\bar{t}g*})_{asym}}{\overline{|\mathcal{M}_{\mathcal{O}(\alpha_s\sqrt{\alpha_s})}^{t\bar{t}g}|_{asym}^2}} = \frac{F_{QED}^{t\bar{t}g}(\alpha_s, \alpha, Q_t, Q_q)}{F_{QCD}^{t\bar{t}g}(\alpha_s)}, \quad (10)$$

$$\frac{\overline{|\mathcal{M}^{t\bar{t}\gamma}|_{\mathcal{O}(\alpha_s^2\alpha),asym}^2}}{\overline{|\mathcal{M}^{t\bar{t}g}|_{\mathcal{O}(\alpha_s^3),asym}^2}} = \frac{\overline{|\mathcal{M}_{\mathcal{O}(\alpha_s\sqrt{\alpha})}^{t\bar{t}\gamma}|_{asym}^2}}{\overline{|\mathcal{M}_{\mathcal{O}(\alpha_s\sqrt{\alpha_s})}^{t\bar{t}g}|_{asym}^2}} = \frac{F_{QED}^{t\bar{t}\gamma}(\alpha_s, \alpha, Q_t, Q_q)}{F_{QCD}^{t\bar{t}g}(\alpha_s)}. \quad (11)$$

$F_{QCD}^{t\bar{t}g}$, $F_{QED}^{t\bar{t}g}$ and $F_{QED}^{t\bar{t}\gamma}$ are related to $F_{QCD}^{t\bar{t}}$, $F_{QED}^{t\bar{t}}$ in the following way,

$$F_{QCD}^{t\bar{t}g} = F_{QCD}^{t\bar{t}}, \quad F_{QED}^{t\bar{t}g} = \frac{2}{3}F_{QED}^{t\bar{t}}, \quad F_{QED}^{t\bar{t}\gamma} = \frac{1}{3}F_{QED}^{t\bar{t}}, \quad (12a)$$

$$F_{QED}^{t\bar{t}} = F_{QED}^{t\bar{t}g} + F_{QED}^{t\bar{t}\gamma}. \quad (12b)$$

This guarantees the cancellation of the IR singularities stemming from the virtual contributions.

The $\mathcal{O}(\alpha_s^2\alpha)$ antisymmetric term from $q\bar{q} \rightarrow t\bar{t}g$ comes from the interference of $q\bar{q} \rightarrow g \rightarrow t\bar{t}g$ (Figure 3) and $q\bar{q} \rightarrow \gamma \rightarrow t\bar{t}g$ (Figure 5). It can be obtained from the corresponding QCD result with the replacement of one gluon by a photon and the right couplings, as done in the case of $q\bar{q} \rightarrow t\bar{t}$. The only difference is the number of gluons to be replaced: in the $q\bar{q} \rightarrow t\bar{t}g$ case they are only two instead of three as for the virtual photon contributions.

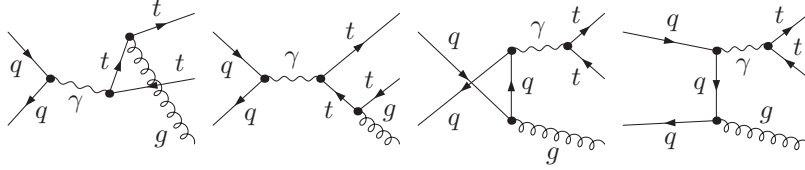


Figure 5: Real gluon emission from photon exchange diagrams

The $\mathcal{O}(\alpha_s^2\alpha)$ antisymmetric term from $q\bar{q} \rightarrow t\bar{t}\gamma$ comes from the $q\bar{q} \rightarrow g \rightarrow t\bar{t}\gamma$ diagrams in Figure 6, and again it can be obtained from the corresponding QCD result for the gluon-radiation process $q\bar{q} \rightarrow t\bar{t}g$. Here we have a one-to-one relation between the QED and QCD diagrams.

Finally, we can relate the QED contribution to the antisymmetric term \tilde{N}_1 in (6) to the $\mathcal{O}(\alpha_s^3)$ QCD term N_1 for a given quark species $q\bar{q} \rightarrow t\bar{t} + X$ in the following way,

$$R_{QED}(Q_q) = \frac{\alpha\tilde{N}_1^{QED}}{\alpha_s N_1} = \frac{F_{QED}^{t\bar{t}}}{F_{QCD}^{t\bar{t}}} = Q_q Q_t \frac{36}{5} \frac{\alpha}{\alpha_s}. \quad (13)$$

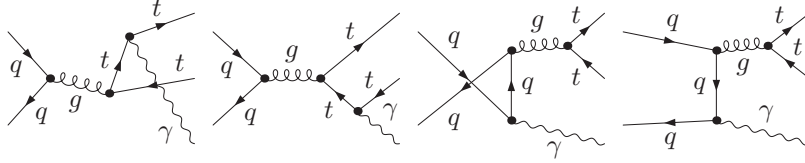


Figure 6: Real photon emission from gluon exchange diagrams

Now we consider the weak contribution to \tilde{N}_1 . It can be depicted by the same diagrams as for $q\bar{q} \rightarrow t\bar{t}$ and $q\bar{q} \rightarrow t\bar{t}g$ in the QED case, but with the photon now substituted by a Z boson, involving massive box diagrams. The result cannot be expressed immediately in a simple factorized way. We performed the explicit calculation including also the contribution from real gluon radiation with numerical integration over the hard gluon part.

Basically also Z -boson radiation, $q\bar{q} \rightarrow t\bar{t}Z$, can contribute at the same order. As our calculation has shown, it yields only a tiny effect of 10^{-5} in A_{FB} and thus may be safely neglected. The same applies to $u\bar{d} \rightarrow t\bar{t}W^+$ as well as to Higgs-boson radiation.

Weak one-loop contributions to the $q\bar{q}g$ and $t\bar{t}g$ vertices induce also axialvector form factors, which however yield vanishing interference terms with the Born amplitude for the antisymmetric cross section at $\mathcal{O}(\alpha_s^2\alpha)$ and are thus irrelevant.

3 Numerical results

The numerical analysis is based on the analytical evaluation of the required symmetric and antisymmetric parts of the parton cross sections and semi-numerical phase-space integration for the radiation processes with phase-space slicing, with support of *FeynArts* [21] and *FormCalc* [22]. This is done also for the QED subclass starting from the $t\bar{t}$, $t\bar{t}g$ and $t\bar{t}\gamma$ diagrams, for comparison with the QED result obtained from (13), showing perfect compatibility.

We choose MRST2004QED parton distributions [23] for NLO calculations and MRST2001LO for LO [24], using thereby $\alpha_s(\mu)$ of MRST2004QED also for the evaluation of the cross sections at LO (a similar strategy was employed in [6]). The same value μ is used also for the factorization scale. The numerical results are presented with three different choices for the scale: $\mu = m_t/2, m_t, 2m_t$. Other input parameters are taken from [25].

The results for the cross sections from the individual partonic channels and their sum, yielding the denominator of A_{FB} , are listed in Table 1. The various antisymmetric terms entering the numerator of either of the two variants $A_{FB}^{t\bar{t}}$ and $A_{FB}^{p\bar{p}}$ are collected in Table 3, and the corresponding contributions to the asymmetry in Table 4.

As already mentioned, the QED part was obtained in two different ways based on the diagrammatic calculation and on the use of (13); the weak part results exclusively from the diagrammatic calculation. The ratio of the total $\mathcal{O}(\alpha_s^2\alpha) + \mathcal{O}(\alpha^2)$ and $\mathcal{O}(\alpha_s^3)$ contributions to the numerator N of the asymmetry (6) gives an illustration of the impact of the electroweak relative to the QCD asymmetry. The values obtained numerically for $\mu = (m_t/2, m_t, 2m_t)$ for the two definitions of

$\sigma(\text{pb})$	$\mu = m_t/2$	$\mu = m_t$	$\mu = 2m_t$
$u\bar{u}$	6.245	4.454	3.355
$d\bar{d}$	1.112	0.777	0.575
$s\bar{s}$	1.37×10^{-2}	9.60×10^{-3}	0.706×10^{-2}
$c\bar{c}$	2.24×10^{-3}	1.69×10^{-3}	1.32×10^{-3}
gg	0.617	0.378	0.248
$p\bar{p}$	7.990	5.621	4.187

Table 1: Integrated cross sections at $\mathcal{O}(\alpha_s^2)$ from the various partonic channels

A_{FB} are

$$\begin{aligned}
R_{EW}^{t\bar{t}} &= \frac{N_{\mathcal{O}(\alpha_s^2\alpha)+\mathcal{O}(\alpha^2)}^{t\bar{t}}}{N_{\mathcal{O}(\alpha_s^3)}^{t\bar{t}}} = (0.190, 0.220, 0.254), \\
R_{EW}^{p\bar{p}} &= \frac{N_{\mathcal{O}(\alpha_s^2\alpha)+\mathcal{O}(\alpha^2)}^{p\bar{p}}}{N_{\mathcal{O}(\alpha_s^3)}^{p\bar{p}}} = (0.186, 0.218, 0.243),
\end{aligned} \tag{14}$$

which are larger than the estimate of 0.09 given in [5]. This shows that the electroweak contribution provides a non-negligible fraction of the QCD-based antisymmetric cross section with the same overall sign, thus enlarging the Standard Model prediction for the asymmetry (the electroweak $\mathcal{O}(\alpha_s^2\alpha)$ contribution of $u\bar{u} \rightarrow t\bar{t}$ to the asymmetry is even bigger than the $\mathcal{O}(\alpha_s^3)$ contribution of $d\bar{d} \rightarrow t\bar{t}$).

The final result for the two definitions of A_{FB} can be summarized as follows,

$$A_{FB}^{t\bar{t}} = (9.7, 8.9, 8.3)\%, \quad A_{FB}^{p\bar{p}} = (6.4, 5.9, 5.4)\%. \tag{15}$$

Figure 7 displays the theoretical prediction versus the experimental data. The prediction is almost inside the experimental 1σ range for $A_{FB}^{t\bar{t}}$ and inside the 2σ range for $A_{FB}^{p\bar{p}}$. It is important to note that the band indicating the scale variation of the prediction does not account for all the theoretical uncertainties. For example, the $\mathcal{O}(\alpha_s^4)$ term in N is missing, and we did not include the $\mathcal{O}(\alpha_s^3)$ part in D . Including the NLO term for the cross section in D would decrease the asymmetry by about 30%, which indicates the size of the NLO terms. In a conservative spirit one would consider this as an uncertainty from the incomplete NLO calculation (see also the discussion in [5]).

We have performed our analysis also for applying two different types of cuts, one to the $t\bar{t}$ invariant mass and the other one to the rapidity: $M_{t\bar{t}} > 450$ GeV and $|\Delta y| > 1$. With those cuts, experimental data have also been presented in [3]. The cross section values for these cuts at LO are given in Table 2. The various terms of the antisymmetric cross section contributing to N , as

$\sigma(\text{pb})$	$\mu = m_t/2$	$\mu = m_t$	$\mu = 2m_t$
$p\bar{p}(M_{t\bar{t}} > 450 \text{ GeV})$	3.113	2.148	1.573
$p\bar{p}(\Delta y > 1)$	1.846	1.276	0.937

Table 2: Cross sections with cuts at $\mathcal{O}(\alpha_s^2)$

discussed above in the case without cuts, are now calculated for $A_{FB}^{t\bar{t}}$ for both cases $M_{t\bar{t}} > 450$ GeV

and $|\Delta y| > 1$. The corresponding contributions to the asymmetry $A_{FB}^{t\bar{t}}$ are the entries of Table 5. The asymmetry with cuts is the total result,

$$A_{FB}^{t\bar{t}}(M_{t\bar{t}} > 450 \text{ GeV}) = (13.9, 12.8, 11.9)\%, \quad A_{FB}^{t\bar{t}}(|\Delta y| > 1) = (20.7, 19.1, 17.5)\%. \quad (16)$$

A comparison of Table 5 with Table 3(a) shows that the ratio of the QCD contribution to the $u\bar{u} \rightarrow t\bar{t}$ and $d\bar{d} \rightarrow t\bar{t}$ subprocesses is larger with the $M_{t\bar{t}} > 450 \text{ GeV}$ cut, which leads to a slight increase of $R_{EW}^{t\bar{t}}$:

$$R_{EW}^{t\bar{t}}(M_{t\bar{t}} > 450 \text{ GeV}) = (0.200, 0.232, 0.266) \quad R_{EW}^{t\bar{t}}(|\Delta y| > 1) = (0.191, 0.216, 0.246). \quad (17)$$

It is, however, not enough to improve the situation.

Figure 8 displays the theoretical prediction versus data for $A_{FB}^{t\bar{t}}$ with cuts. The Standard Model prediction is inside the 2σ range for the $|\Delta y| > 1$ cut, but it is at the 3σ boundary for the invariant-mass cut $M_{t\bar{t}} > 450 \text{ GeV}$.

4 Conclusions

Our detailed analysis of the electroweak contributions to the forward-backward asymmetry in $t\bar{t}$ production shows that they provide a non-negligible fraction of the QCD-induced asymmetry with the same overall sign, thus enlarging the Standard Model prediction for the asymmetry at the Tevatron. For high invariant masses, a 3σ deviation from the measured value still persists. The observed dependence of A_{FB} on the invariant mass of $t\bar{t}$ could be an indication for the presence of new physics below the TeV scale; it is, however, difficult to interpret these deviations as long as the NLO QCD calculation for the asymmetry is not available.

(a) $A_{FB}^{t\bar{t}}$

$N(\text{pb})$	$\mu = m_t/2$	$\mu = m_t$	$\mu = 2m_t$
$\mathcal{O}(\alpha_s^3) \quad u\bar{u}$	0.560	0.354	0.234
$\mathcal{O}(\alpha_s^3) \quad d\bar{d}$	9.25×10^{-2}	5.76×10^{-2}	3.76×10^{-2}
$\mathcal{O}(\alpha_s^2\alpha)_{QED} \quad u\bar{u}$	0.108	0.0759	0.0554
$\mathcal{O}(\alpha_s^2\alpha)_{QED} \quad d\bar{d}$	-8.9×10^{-3}	-6.2×10^{-3}	-4.5×10^{-3}
$\mathcal{O}(\alpha_s^2\alpha)_{weak} \quad u\bar{u}$	1.25×10^{-2}	0.89×10^{-2}	0.66×10^{-2}
$\mathcal{O}(\alpha_s^2\alpha)_{weak} \quad d\bar{d}$	-3.6×10^{-3}	-2.5×10^{-3}	-1.8×10^{-3}
$\mathcal{O}(\alpha^2) \quad u\bar{u}$	1.47×10^{-2}	1.30×10^{-2}	1.17×10^{-2}
$\mathcal{O}(\alpha^2) \quad d\bar{d}$	1.8×10^{-3}	1.6×10^{-3}	1.4×10^{-3}

(b) $A_{FB}^{p\bar{p}}$

$N(\text{pb})$	$\mu = m_t/2$	$\mu = m_t$	$\mu = 2m_t$
$\mathcal{O}(\alpha_s^3) \quad u\bar{u}$	0.373	0.236	0.155
$\mathcal{O}(\alpha_s^3) \quad d\bar{d}$	5.97×10^{-2}	3.72×10^{-2}	2.42×10^{-2}
$\mathcal{O}(\alpha_s^2\alpha)_{QED} \quad u\bar{u}$	7.15×10^{-2}	5.06×10^{-2}	3.67×10^{-2}
$\mathcal{O}(\alpha_s^2\alpha)_{QED} \quad d\bar{d}$	-5.7×10^{-3}	-4.0×10^{-3}	-2.9×10^{-3}
$\mathcal{O}(\alpha_s^2\alpha)_{weak} \quad u\bar{u}$	8.2×10^{-3}	5.8×10^{-3}	4.2×10^{-3}
$\mathcal{O}(\alpha_s^2\alpha)_{weak} \quad d\bar{d}$	-2.3×10^{-3}	-1.6×10^{-3}	-1.1×10^{-3}
$\mathcal{O}(\alpha^2) \quad u\bar{u}$	9.1×10^{-3}	8.0×10^{-3}	7.1×10^{-3}
$\mathcal{O}(\alpha^2) \quad d\bar{d}$	1.1×10^{-3}	1.0×10^{-3}	0.9×10^{-3}

Table 3: The various contributions to the antisymmetric cross section N of $A_{FB}^{t\bar{t}}$ and $A_{FB}^{p\bar{p}}$

(a) $A_{FB}^{t\bar{t}}$				(b) $A_{FB}^{p\bar{p}}$			
$A_{FB}^{t\bar{t}}$	$\mu = m_t/2$	$\mu = m_t$	$\mu = 2m_t$	$A_{FB}^{p\bar{p}}$	$\mu = m_t/2$	$\mu = m_t$	$\mu = 2m_t$
$\mathcal{O}(\alpha_s^3) u\bar{u}$	7.01%	6.29%	5.71%	$\mathcal{O}(\alpha_s^3) u\bar{u}$	4.66%	4.19%	3.78%
$\mathcal{O}(\alpha_s^3) d\bar{d}$	1.16%	1.03%	0.92%	$\mathcal{O}(\alpha_s^3) d\bar{d}$	0.75%	0.66%	0.59%
$\mathcal{O}(\alpha_s^2\alpha)_{QED} u\bar{u}$	1.35%	1.35%	1.35%	$\mathcal{O}(\alpha_s^2\alpha)_{QED} u\bar{u}$	0.90%	0.90%	0.90%
$\mathcal{O}(\alpha_s^2\alpha)_{QED} d\bar{d}$	-0.11%	-0.11%	-0.11%	$\mathcal{O}(\alpha_s^2\alpha)_{QED} d\bar{d}$	-0.07%	-0.07%	-0.07%
$\mathcal{O}(\alpha_s^2\alpha)_{weak} u\bar{u}$	0.16%	0.16%	0.16%	$\mathcal{O}(\alpha_s^2\alpha)_{weak} u\bar{u}$	0.10%	0.10%	0.10%
$\mathcal{O}(\alpha_s^2\alpha)_{weak} d\bar{d}$	-0.04%	-0.04%	-0.04%	$\mathcal{O}(\alpha_s^2\alpha)_{weak} d\bar{d}$	-0.03%	-0.03%	-0.03%
$\mathcal{O}(\alpha^2) u\bar{u}$	0.18%	0.23%	0.28%	$\mathcal{O}(\alpha^2) u\bar{u}$	0.11%	0.14%	0.17%
$\mathcal{O}(\alpha^2) d\bar{d}$	0.02%	0.03%	0.03%	$\mathcal{O}(\alpha^2) d\bar{d}$	0.01%	0.02%	0.02%
tot $p\bar{p}$	9.72%	8.93%	8.31%	tot $p\bar{p}$	6.42%	5.92%	5.43%

Table 4: Individual and total contributions to $A_{FB}^{t\bar{t}}$ and $A_{FB}^{p\bar{p}}$

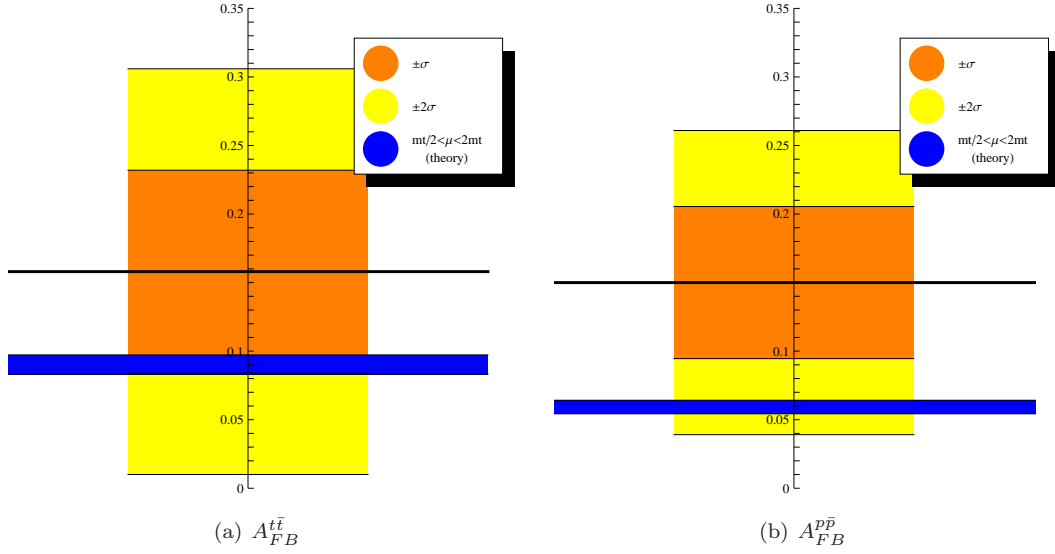


Figure 7: Theory(blue) and experimental data (black=central value, orange= 1σ , yellow= 2σ)

(a) $A_{FB}^{t\bar{t}}(M_{t\bar{t}} > 450 \text{ GeV})$				(b) $A_{FB}^{t\bar{t}}(\Delta y > 1)$			
$A_{FB}^{t\bar{t}}$	$\mu = m_t/2$	$\mu = m_t$	$\mu = 2m_t$	$A_{FB}^{t\bar{t}}$	$\mu = m_t/2$	$\mu = m_t$	$\mu = 2m_t$
$\mathcal{O}(\alpha_s^3) u\bar{u}$	10.13%	9.10%	8.27%	$\mathcal{O}(\alpha_s^3) u\bar{u}$	15.11%	13.72%	12.41%
$\mathcal{O}(\alpha_s^3) d\bar{d}$	1.44%	1.27%	1.14%	$\mathcal{O}(\alpha_s^3) d\bar{d}$	2.28%	2.02%	1.84%
$\mathcal{O}(\alpha_s^2\alpha)_{QED} u\bar{u}$	1.94%	1.95%	1.96%	$\mathcal{O}(\alpha_s^2\alpha)_{QED} u\bar{u}$	2.90%	2.94%	2.94%
$\mathcal{O}(\alpha_s^2\alpha)_{QED} d\bar{d}$	-0.14%	-0.14%	-0.14%	$\mathcal{O}(\alpha_s^2\alpha)_{QED} d\bar{d}$	-0.22%	-0.22%	-0.22%
$\mathcal{O}(\alpha_s^2\alpha)_{weak} u\bar{u}$	0.28%	0.28%	0.28%	$\mathcal{O}(\alpha_s^2\alpha)_{weak} u\bar{u}$	0.25%	0.25%	0.26%
$\mathcal{O}(\alpha_s^2\alpha)_{weak} d\bar{d}$	-0.05%	-0.05%	-0.05%	$\mathcal{O}(\alpha_s^2\alpha)_{weak} d\bar{d}$	-0.09%	-0.09%	-0.08%
$\mathcal{O}(\alpha^2) u\bar{u}$	0.26%	0.33%	0.41%	$\mathcal{O}(\alpha^2) u\bar{u}$	0.35%	0.45%	0.55%
$\mathcal{O}(\alpha^2) d\bar{d}$	0.03%	0.03%	0.04%	$\mathcal{O}(\alpha^2) d\bar{d}$	0.04%	0.05%	0.06%
tot $p\bar{p}$	13.90%	12.77%	11.91%	tot $p\bar{p}$	20.70%	19.12%	17.75%

Table 5: Individual and total contributions to $A_{FB}^{t\bar{t}}(M_{t\bar{t}} > 450 \text{ GeV})$ and $A_{FB}^{t\bar{t}}(|\Delta y| > 1)$

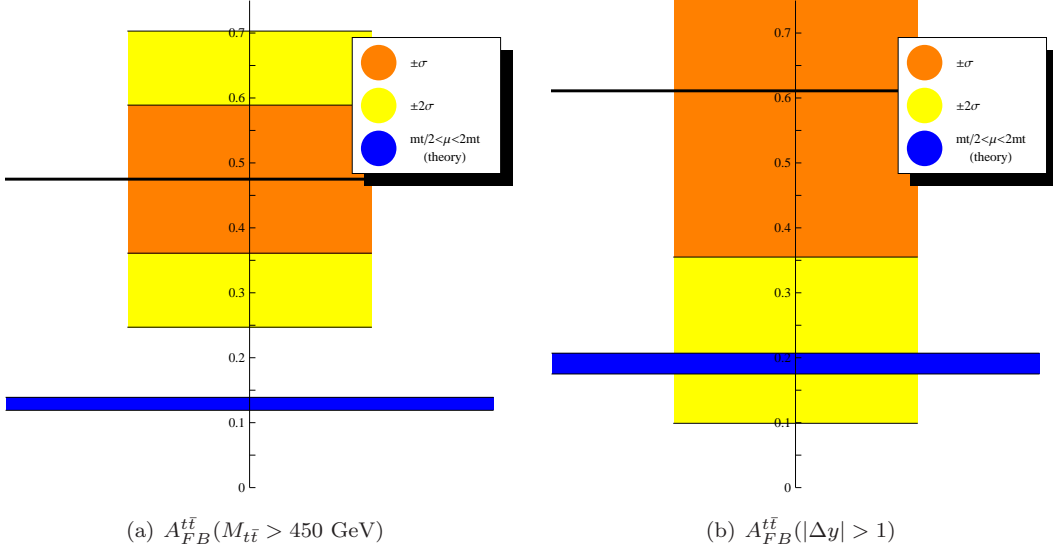


Figure 8: Theory(blue) and experimental data (black=central value, orange= 1σ , yellow= 2σ)

References

- [1] **CDF** Collaboration, T. Aaltonen *et. al.*, *Forward-Backward Asymmetry in Top Quark Production in $p\bar{p}$ Collisions at $\sqrt{s}=1.96$ TeV*, *Phys.Rev.Lett.* **101** (2008) 202001, [[arXiv:0806.2472](#)].
- [2] **D0** Collaboration, S.-J. Park, *Measurement of the Forward-Backward Charge Asymmetry in Top-Quark Pair Production in Proton-Antiproton Collisions at D0*, *AIP Conf.Proc.* **1078** (2009) 590–592, [[arXiv:0810.4751](#)].
- [3] **CDF** Collaboration, T. Aaltonen *et. al.*, *Evidence for a Mass Dependent Forward-Backward Asymmetry in Top Quark Pair Production*, [arXiv:1101.0034](#).
- [4] J. H. Kuhn and G. Rodrigo, *Charge asymmetry in hadroproduction of heavy quarks*, *Phys.Rev.Lett.* **81** (1998) 49–52, [[hep-ph/9802268](#)].
- [5] J. H. Kuhn and G. Rodrigo, *Charge asymmetry of heavy quarks at hadron colliders*, *Phys.Rev.* **D59** (1999) 054017, [[hep-ph/9807420](#)].
- [6] W. Bernreuther and Z.-G. Si, *Distributions and correlations for top quark pair production and decay at the Tevatron and LHC.*, *Nucl.Phys.* **B837** (2010) 90–121, [[arXiv:1003.3926](#)].
- [7] G. Rodrigo and P. Ferrario, *Charge asymmetry: A Theory appraisal*, *Nuovo Cim.* **C33** (2010) 04, [[arXiv:1007.4328](#)].
- [8] J. Shu, K. Wang, and G. Zhu, *A Revisit to Top Quark Forward-Backward Asymmetry*, [arXiv:1104.0083](#).
- [9] M. Gluck, J. Owens, and E. Reya, *Gluon Contribution to Hadronic J/psi Production*, *Phys.Rev.* **D17** (1978) 2324.
- [10] B. Combridge, *Associated Production of Heavy Flavor States in $p p$ and $anti-p p$ Interactions: Some QCD Estimates*, *Nucl.Phys.* **B151** (1979) 429.
- [11] J. Babcock, D. W. Sivers, and S. Wolfram, *QCD Estimates for Heavy Particle Production*, *Phys.Rev.* **D18** (1978) 162.
- [12] K. Hagiwara and T. Yoshino, *Hadroproduction of Heavy Quark Flavors in QCD*, *Phys.Lett.* **B80** (1979) 282.
- [13] L. Jones and H. Wyld, *On Hadronic Charm Production by Gluon Fusion*, *Phys.Rev.* **D17** (1978) 1782.
- [14] H. Georgi, S. Glashow, M. Machacek, and D. V. Nanopoulos, *Charmed Particles from two - Gluon Annihilation in Proton Proton Collisions*, *Annals Phys.* **114** (1978) 273.
- [15] P. Nason, S. Dawson, and R. Ellis, *The Total Cross-Section for the Production of Heavy Quarks in Hadronic Collisions*, *Nucl.Phys.* **B303** (1988) 607.
- [16] G. Altarelli, M. Diemoz, G. Martinelli, and P. Nason, *Total Cross-Sections for Heavy Flavor Production in Hadronic Collisions and QCD*, *Nucl.Phys.* **B308** (1988) 724.

- [17] W. Beenakker, H. Kuijf, W. van Neerven, and J. Smith, *QCD Corrections to Heavy Quark Production in p anti- p Collisions*, *Phys.Rev.* **D40** (1989) 54–82.
- [18] K. Melnikov and M. Schulze, *NLO QCD corrections to top quark pair production and decay at hadron colliders*, *JHEP* **0908** (2009) 049, [[arXiv:0907.3090](#)].
- [19] V. Ahrens, A. Ferroglia, M. Neubert, B. D. Pecjak, and L. L. Yang, *RG-improved single-particle inclusive cross sections and forward-backward asymmetry in $t\bar{t}$ production at hadron colliders*, [arXiv:1103.0550](#).
- [20] V. Ahrens, A. Ferroglia, M. Neubert, B. D. Pecjak, and L. L. Yang, *The top-pair forward-backward asymmetry beyond NLO*, [arXiv:1106.6051](#).
- [21] T. Hahn, *Generating Feynman diagrams and amplitudes with FeynArts 3*, *Comput.Phys.Commun.* **140** (2001) 418–431, [[hep-ph/0012260](#)].
- [22] T. Hahn and M. Perez-Victoria, *Automatized one loop calculations in four-dimensions and D-dimensions*, *Comput.Phys.Commun.* **118** (1999) 153–165, [[hep-ph/9807565](#)].
- [23] A. Martin, R. Roberts, W. Stirling, and R. Thorne, *Parton distributions incorporating QED contributions*, *Eur.Phys.J.* **C39** (2005) 155–161, [[hep-ph/0411040](#)].
- [24] A. Martin, R. Roberts, W. Stirling, and R. Thorne, *NNLO global parton analysis*, *Phys.Lett.* **B531** (2002) 216–224, [[hep-ph/0201127](#)].
- [25] **Particle Data Group** Collaboration, K. Nakamura *et. al.*, *Review of particle physics*, *J.Phys.G* **G37** (2010) 075021.